Total Ionizing Dose and Proton Radiation Characterization of Si P-i-N Visible Hybrid Focal Plane Arrays

John E. Hubbs*[a], Mark E. Gramer[a] , Douglas C. Arrington[a], Gary A. Dole[a], Diana Maestas-Jepson[a]
Sheldon E. Takeall[b]
[a]Air Force Research Laboratory/Space Vehicles Directorate, Infrared Radiation Effects Laboratory, Ball Aerospace & Technologies Corp., P.O. Box 5209, Albuquerque, New Mexico 87185
[b]Air Force Research Laboratory/Space Vehicles Directorate, 3750 Sherman Avenue, S.E. Kirtland Air Force Base, New Mexico 87117

ABSTRACT

The results of total ionizing dose and proton fluence characterization of hybrid Si P-i-N focal plane arrays are reported. The focal plane arrays consist of a silicon P-i-N detector array bump bonded to 128 x 128 CMOS readout integrated circuit (ROIC). The FPAs were characterized in total ionizing dose and proton fluence radiation environments. Full radiometric characterizations were performed at each radiation dose level to determine the impact of the radiation on dark current, noise, responsivity, sensitivity, and dynamic range. Results from the total ionizing dose experiment demonstrate an unexpected increase in the visible P-i-N detector dark current. The median dark current increased more than two orders of magnitude from pre-radiation to 300 krad(Si) and the magnitude of the dark current was found to be a strong function of detector bias. No appreciable change in responsivity or noise was observed for wavelengths above 400 nm up to a total ionizing dose of 750 krad(Si). Results from the proton radiation experiment show no appreciable change in responsivity was observed up to a 63 MeV proton fluence of 3 x 10^{12} protons/cm^2 (400 krad(Si) of total ionizing dose). The median dark current increased approximately two orders of magnitude, but even at this higher level, the dark current did not contribute significantly to the median noise at an integration time of 10 ms. The dominant degradation mechanism, in both the total ionizing dose and proton fluence environments, is an increase in dark current in the Si P-i-N detectors.

Keywords: Si P-i-N Detectors, CMOS, Proton Fluence, Total Ionizing Dose

1. INTRODUCTION

Space-based imaging applications place stringent performance requirements on focal plane arrays (FPAs) in terms of sensitivity, uniformity, operability, and radiation hardness. The high radiation requirements that are being placed on FPAs for NASA space-based imaging applications cannot be accommodated using charge coupled devices (CCDs)[1,2,3]; therefore, a new type of FPA is required to meet these requirements. One of the many technologies being pursued to fill this requirement is a hybrid focal plane array that mates a Si P-i-N detector array with a readout integrated circuit (ROIC). This approach offers the advantage of being able to independently optimize the performance of the detector array and the ROIC before mating to form the FPA. This technology leverages heavily from advances in the infrared focal plane industry where radiation hardening of focal plane arrays is, in general, a more mature concept. This paper reports on the results of radiometric, total ionizing dose and proton fluence radiation characterizations of visible hybrid FPAs.

The FPAs described in this paper were developed to demonstrate the radiation tolerance of the visible Si P-i-N hybrid FPA technology. The ROIC utilized in this study was originally developed for use in space based infrared systems operating at deep cryogenic temperatures and was selected because of its proven tolerance to total ionizing radiation. The format of the FPA was dictated by the availability of this radiation tolerant ROIC. Manufacturers are accustomed to fabricating very large format FPAs with the visible P-i-N hybrid FPA technology. For this study, two visible hybrid FPAs were characterized using Cobalt-60 radiation to produce total ionizing dose damage. Operational and performance data were obtained on both devices as a function of total dose up to a dose of 750 krad(Si). Two additional visible hybrid FPAs were characterized in a 63 MeV proton radiation environment that produces both displacement and

* jhubbs@ieee.org; phone 1-505-846-6627;

Focal Plane Arrays for Space Telescopes II, edited by Thomas J. Grycewicz, Cheryl J. Marshall,
Proceedings of SPIE Vol. 5902 (SPIE, Bellingham, WA, 2005) · 0277-786X/05/$15 · doi: 10.1117/12.625538

ionizing damage to the FPAs. Operational and performance data were obtained as a function of 63 MeV proton fluence. The main performance metrics evaluated as a function of radiation dose for the FPA were the sensitivity, which is quantified by the Noise Equivalent Irradiance (NEI), the detector spectral response which is quantified by the FPA responsivity as a function of wavelength, and the detector dark current. The measurement of the detector spectral response as a function of radiation level was an important element of these characterizations.

The remainder of this paper is divided into four sections: Section 2 gives a description of the visible hybrid FPAs; Section 3 discusses the measurements and analyses performed on the data; and Section 4 presents the characterization data obtained for each device.

2. DESCRIPTION OF VISIBLE FOCAL PLANE ARRAYS

These hybrid visible FPAs were designed to meet stringent performance requirements for space based imaging applications. Si P-i-N detector technology, in a 128 x 128 format with a 60-µm-detector pitch, is utilized in these visible hybrid FPAs. The detectors have an anti-reflection (AR) coating to improve their short wavelength response.

The ROIC utilizes a capacitive transimpedance amplifier (CTIA) unit cell with on-chip correlated-double-sampling (CDS). A source follower amplifier, that places the pixel outputs into a pipeline architecture where the signal from one row is stored while the output amplifier is reading the signal from the previous row, buffers the unit cell amplifier. The output amplifier is another source follower with an on-chip load. The ROIC makes extensive use of auto-biasing circuitry to enhance its total ionizing dose radiation hardness. These biases are dynamically changed as the ROIC accumulates total dose radiation, compensating for radiation induced threshold voltage shifts. A functional block diagram of the signal chain is shown in Figure 1.

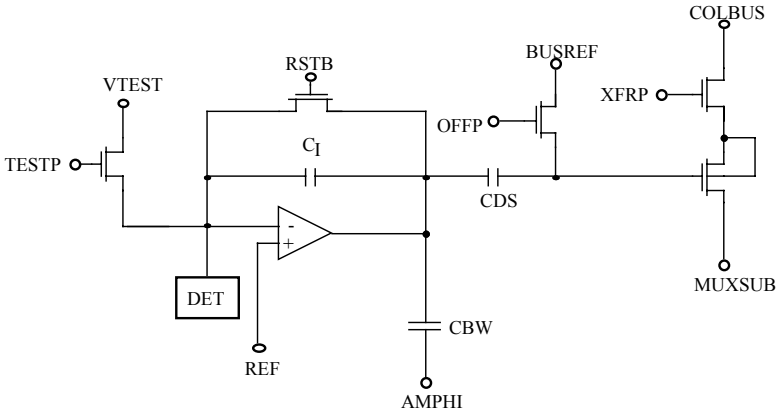

Figure 1. ROIC Signal Chain Functional Diagram.

3. VISIBLE HYBRID FPA RADIOMETRIC PERFORMANCE DATA

The FPAs were radiometrically characterized prior to exposure to radiation. These radiometric data include the FPA responsivity, dynamic range, sensitivity, and dark current are described below.

3.1. FPA RESPONSIVITY

The FPA responsivity is determined by measuring the FPA output as a function of photon irradiance. The total detector current is the sum of the contributions from dark current and photon irradiation. The total detector current and the corresponding FPA pixel output voltage are given in Equations 1 and 2, respectively.

$$I_{total} = q\eta E_q A_{Det} + I_{dark} \tag{1}$$

$$V_{output} = C_g\left(\eta E_q A_{\det}\tau_{\text{int}} + \frac{I_{dark}\tau_{\text{int}}}{q}\right) + V_{offset} \tag{2}$$

where: q = electronic charge (1.6 x 10^{-19} coulombs)
η = quantum efficiency (electrons/photon)
E_q = photon irradiance (ph/s-cm^2)
A_{det} = detector area (cm^2)
C_g = conversion gain (volts/electron)
t_{int} = integration time (seconds)
I_{dark} = total pixel dark current (amps)
V_{offset} = ROIC offset voltage (volts)

In the expression for the detector current, the first term is the current due to the photon irradiance and the second is pixel dark current. Similarly, in the equation for the output voltage, the first term is the output due to the photon irradiance, the second term is due to the pixel dark current, and the third is a constant due to the ROIC. The pixel output voltage is a linear function of the photon irradiance (within the linear range of the readout), as given by Equation 2, and the FPA responsivity is proportional to the slope of output versus irradiance, as expressed in Equation 3. To obtain the responsivity, the values for detector area and integration time are used with Equation 3 and the FPA output measured at different photon irradiance levels. The responsivity reported here is at 650 nm.

$$\text{Responsivity} = C_g\eta = \frac{dV_{Output}}{d\left(E_q A_{\text{det}}\tau_{\text{int}}\right)} = \frac{1}{A_{\text{det}}\tau_{\text{int}}}\frac{dV_{Output}}{d\left(E_q\right)} \quad \left(\frac{Volts}{photon}\right) \tag{3}$$

The ROIC has a measured linear output swing of approximately 1.7 V that corresponds to a well capacity of over 2 x 10^6 electrons. The responsivity histogram and cumulative distribution plots (right scale) for the visible hybrid FPA are shown in Figure 2. It has an uncorrected responsivity non-uniformity (sigma/mean) of approximately 1.3% with an operability, as defined as the percentage of pixels within 25% of the mean responsivity, of 99.95%. The mean responsivity is 178 x 10^{-15} V/photon/sec-cm^2, corresponding to a detector quantum efficiency of 79%, based on a conversion gain of 0.62 µV/electron.

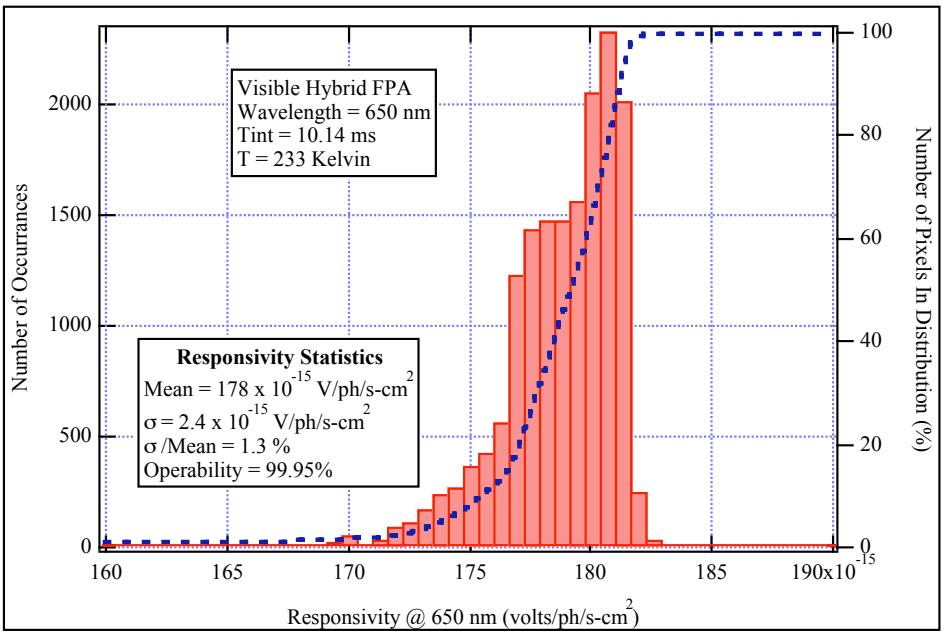

Figure 2. Visible Hybrid FPA Responsivity Distribution.

3.2. FPA SENSITIVITY

The Noise Equivalent Irradiance (NEI) is a measure of the sensitivity of an FPA. It is based on the pixel noise-to-signal ratio as expressed by Equation 4. NEI histograms and cumulative distribution plots (right scale) at different irradiance levels at a temperature of 233 K are shown in Figure 3. Summaries of NEI performance statistics in terms of the uncorrected non-uniformity (σ/mean), operability, defined as the percentage of pixels within 25% of the median NEI, and the absolute NEI level for the median pixel and the 99.95 percentile pixel are given in Table 1. These data indicate a high level of operability, good uniformity, and excellent sensitivity. Median NEI, based on the median pixel noise and responsivity, is shown as a function of photon irradiance in Figure 4. Included with the measured data is a plot of the Background Limited Performance (BLIP) NEI for a detector quantum efficiency of 78%. At low irradiance levels, the NEI is limited by the ROIC read noise and it approaches BLIP at a photon irradiance level of 10^{12} ph/sec-cm^2. At these operating temperatures, the dark current contribution to the FPA noise is insignificant.

$$NEI\left(\frac{photons}{\text{sec}-cm^2}\right) = \frac{RMS\ Noise\ (Volts)}{\text{Responsivity}\left(\frac{Volts}{\frac{photons}{\text{sec}-cm^2}}\right)} \tag{4}$$

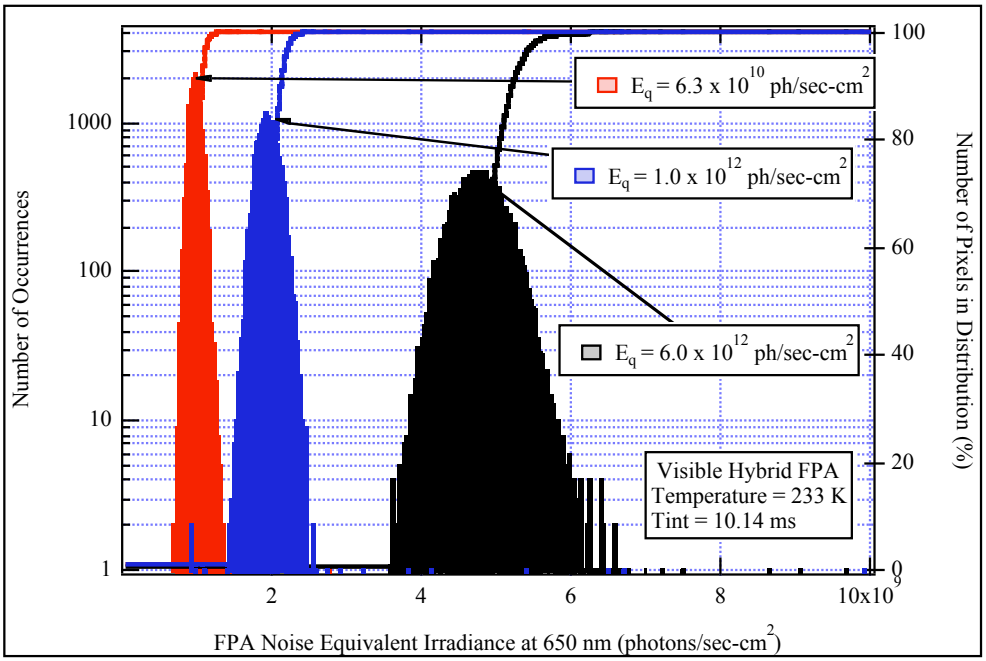

Figure 3. Visible Hybrid FPA NEI Histograms.

Table 1. Summary of Noise Equivalent Irradiance (NEI) Performance Statistics

Visible Hybrid FPA Temperature = 233 K tint = 10.14 ms				
Photon Irradiance (photons/sec-cm^2)	Median NEI (photons/sec-cm^2)	99th Percentile NEI (photons/sec-cm^2)	Operability (%)	Non-Uniformity (%)
6.3 x 10^{10}	9.71 x 10^8	1.21 x 10^9	98.54	11.7
1.0 x 10^{12}	1.92 x 10^9	2.32 x 10^9	98.79	11.4
6.0 x 10^{12}	4.72 x 10^9	5.81 x 10^9	99.32	7.4

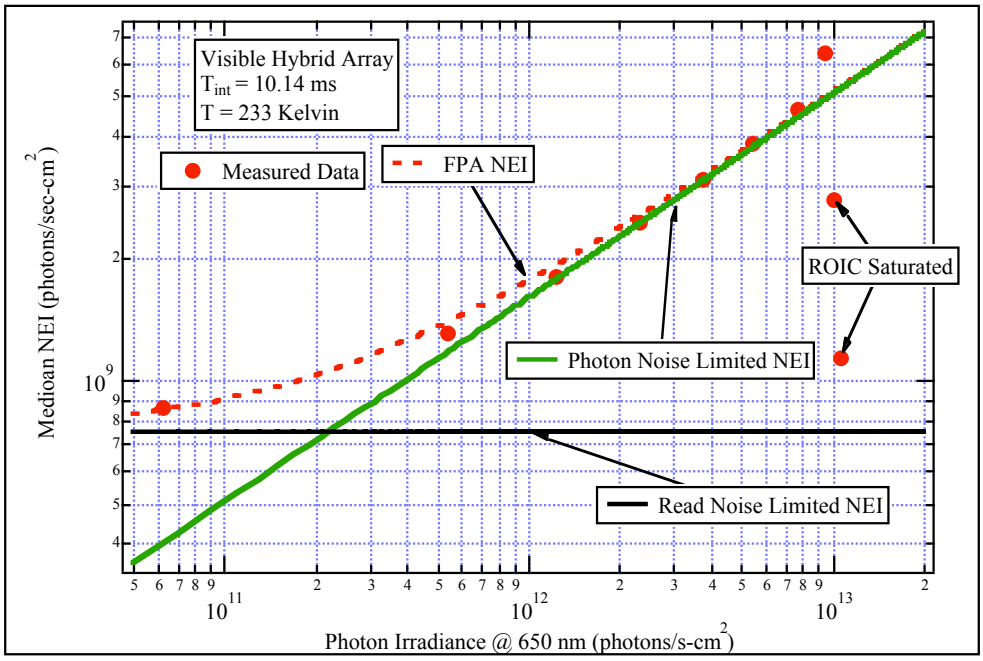

Figure 4. Median Noise Equivalent Irradiance versus Photon Irradiance.

3.3. Si P-i-N Detector Dark Current

The detector dark current is determined by measuring the FPA output as a function of integration time at a very low photon irradiance level. The total detector current is the sum of the contributions from dark current and photon irradiation. To solve for the detector dark current, the expression for output voltage (Equation 2) is differentiated with respect to integration time to yield:

$$\frac{d\left(V_{Output}\right)}{d\left(\tau_{\text{int}}\right)} = C_g \eta E_q A_{\text{det}} + \frac{C_g I_{dark}}{q} = \frac{C_g}{q}\left[\left(\eta e E_q A_{\text{det}}\right) + I_{dark}\right] \tag{5}$$

The first term in the brackets is the pixel current due to the photon irradiance and the second is the dark current. For this measurement, the FPA was placed in the dark; therefore there is no contribution to the FPA output due to photon irradiance. Output voltage measurements were made as a function of integration time and the dark current was then calculated from the slope of these plots and Equation 6.

$$I_{dark}\left(Amps\right) = \frac{q}{C_g}\frac{d\left(V_{Output}\right)}{d\left(\tau_{\text{int}}\right)} \tag{6}$$

The dark current histogram and cumulative distribution plots (right scale) for the visible hybrid FPA at an operating temperature of 233 Kelvin are shown in Figure 5. The mean dark current at 233 Kelvin is 6.43 x 10^{-15} A which corresponds to 40 x 10^{3} electrons/sec. The dark current non-uniformity (sigma/mean) is approximately 6.4%. The median FPA dark current plotted as a function of inverse temperature for a number of detector biases is shown in Figure 6. These data indicate that the dark current has an activation energy of 0.63 eV, except at the lowest detector bias where the activation energy is slightly higher.

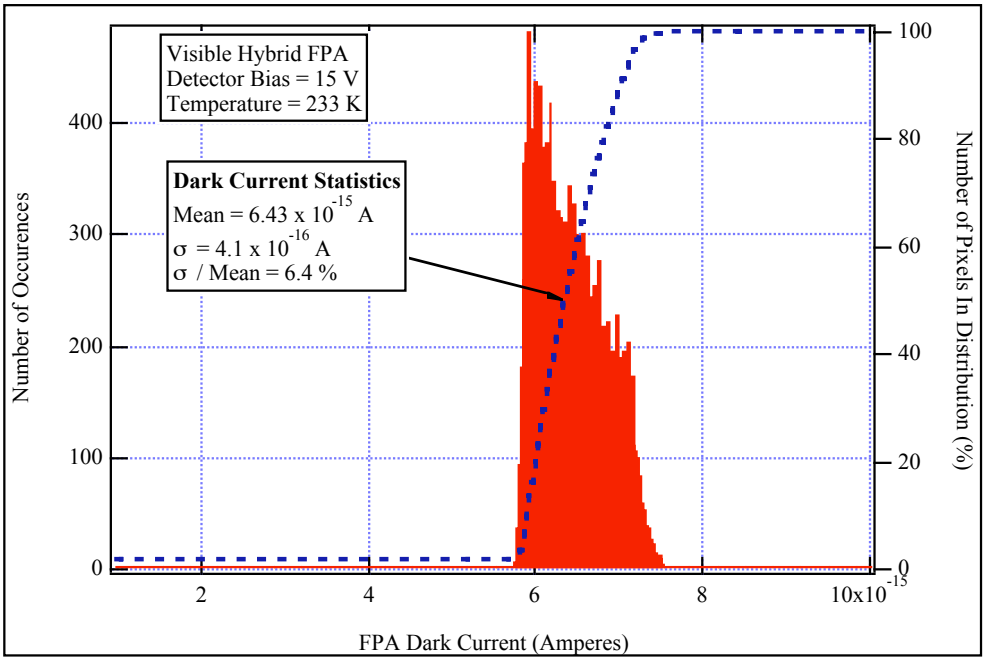

Figure 5. FPA Dark Current Histogram at 233 Kelvin.

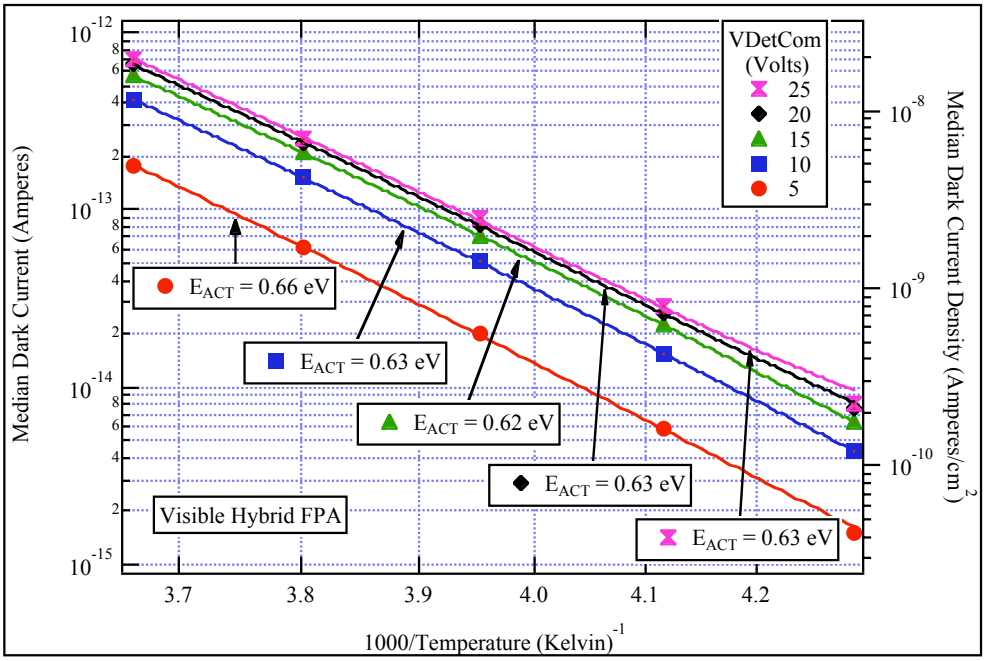

Figure 6. Dark Current versus Inverse Temperature.

4. VISIBLE HYBRID FPA RADIATION CHARACTERIZATION DATA

4.1. FPA Performance versus Proton Fluence

The operational and radiometric performance of the visible hybrid FPA was characterized as a function of proton fluence at the Crocker Nuclear Laboratory (CNL) of the University of California, Davis (UC Davis). The proton beam facility at CNL is based on the 76" Isochronous Cyclotron that can provide protons with energies up to 68 MeV[4]. The beam energy is measured by a time of flight system in combination with knowledge of the cyclotron magnetic field settings. Beam counting is performed by the combination of a Secondary Electron Emission Monitor and a removable Faraday Cup. A Segmented Secondary Electron Emission Monitor positions the proton beam in the center of the target. For these experiments, the cyclotron was configured to irradiate the FPA at 63 MeV, and the FPA was fully biased and operational at 233 K during irradiation. The FPA was mounted at a 45° angle with respect to the proton beam line and to the incident photon irradiance, so that the FPA could simultaneously be illuminated by the photon irradiance and irradiated by protons.

4.1.1. FPA Radiometric Characterization Versus Proton Fluence

The radiometric performance of the FPA was characterized as a function of proton fluence. Significant results observed were: (1) some very slight change in the FPA responsivity; (2) a shift in the nominal pixel dc output level; (3) minor changes in the noise level; and (4) an increase in the NEI non-uniformity at low photon irradiance levels. The radiometric performance as a function of proton fluence is summarized in Figure 7, which plots the median pixel output voltage as a function of photon irradiance at a number of proton fluence levels. These data demonstrate a FPA linearity of better than 1% over a 2 V output voltage range. These data also show that the responsivity, as determined from the slopes of these plots, is relatively constant up to a 63 MeV proton fluence of 3×10^{12} p/cm^2 that corresponds to a total ionizing dose of 400 krad(Si). The average responsivity at 650 nm, as determined from the measured responsivity at each proton fluence, is 1.875×10^{-13} V/ph/s-cm^2 with a standard deviation of 1.3×10^{-15} V/ph/s-cm^2. This result demonstrates that the detector quantum efficiency at 650 nm and the ROIC conversion gain do not change with proton fluence. These data do show a slight shift in the FPA output of approximately 30 mV at a proton fluence of 3×10^{12} p/cm^2 that is due to uncompensated threshold shifts due to the accumulation of total ionizing dose in the ROIC. Responsivity distributions, shown in Figure 8 for both pre-radiation and at the maximum proton fluence of 3.0×10^{12} p/cm^2, show very little change with proton fluence and demonstrate that uniformity of the FPA responsivity is maintained with proton fluence.

One objective of these experiments was to evaluate the detector quantum efficiency (QE) of the Si P-i-N detectors as a function of proton fluence. It was hypothesized that the detector quantum efficiency would degrade, especially at shorter wavelengths, due to a degradation of the minority carrier lifetime with increasing proton fluence. In addition, it was thought that the detector would not remain fully depleted under nominal biasing conditions after proton irradiation, which would further exacerbate the degradation of the detector quantum efficiency. Pre-radiation measurements indicated that the Si P-i-N detectors were fully depleted prior to proton irradiation at a detector substrate bias of 15 V; however, it was thought that higher biases would be required to achieve full depletion after proton irradiation. To investigate these effects, the detector quantum efficiency was measured as a function of detector bias at several wavelengths as a function of proton fluence.

Prior to proton irradiation, the measured FPA responsivity was determined to be independent of detector bias at all wavelengths from near zero volts to 15 V. Median pixel response, normalized to the response at a bias of 40 V, is plotted in Figure 9 at a proton fluence of 3×10^{12} p/cm^2 and show that the FPA responsivity is slightly degraded and the degradation is most extreme at shorter wavelengths. Operating the detector bias at a higher operating point can mitigate the FPA responsivity degradation by ensuring that full depletion has been achieved, which makes the detector quantum efficiency less reliant on the minority carrier lifetime. However, even at the shortest wavelengths, the loss of detector quantum efficiency at a bias of 15 V is less than 5% at a 63 MeV proton fluence of 3×10^{12} p/cm^2.

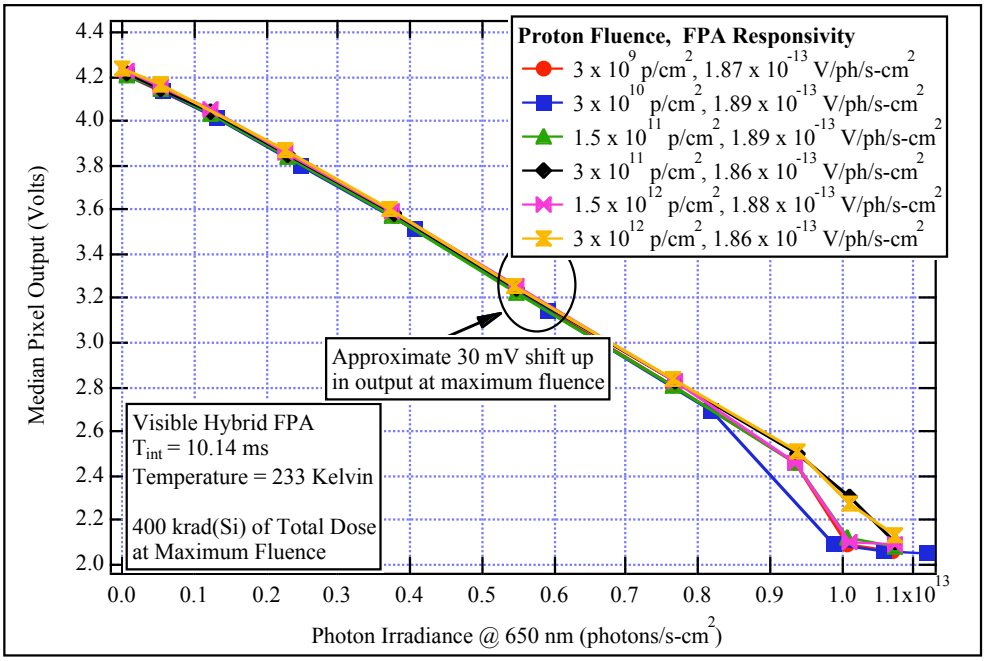

Figure 7. Median FPA Output versus Photon Irradiance at a Different Proton Fluence Levels.

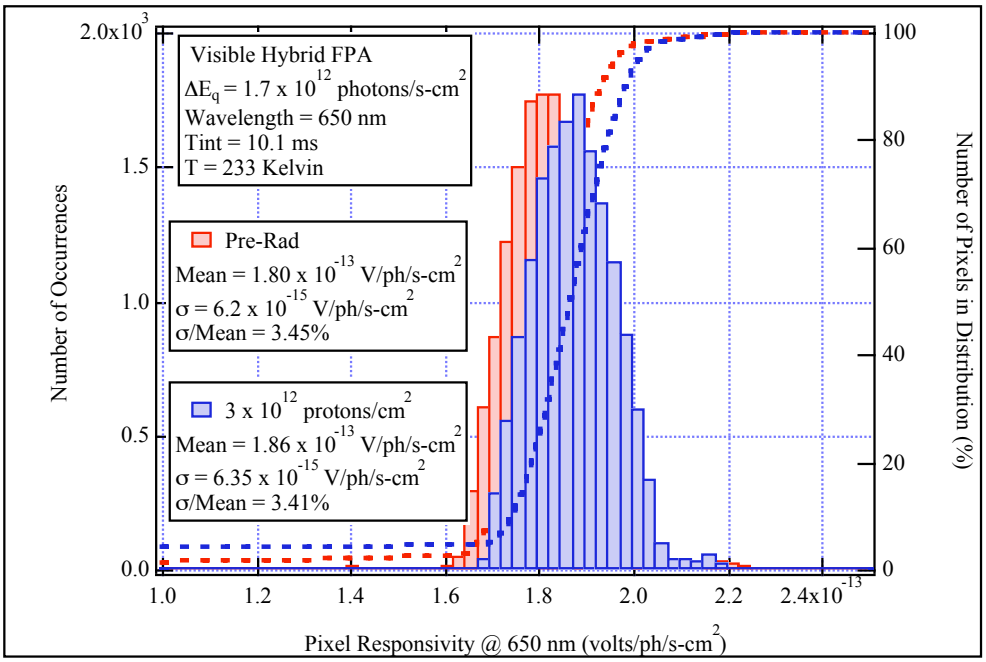

Figure 8. Responsivity Histograms, Pre-Radiation and Proton Fluence = 3.0 x 10^{12} p/cm^2.

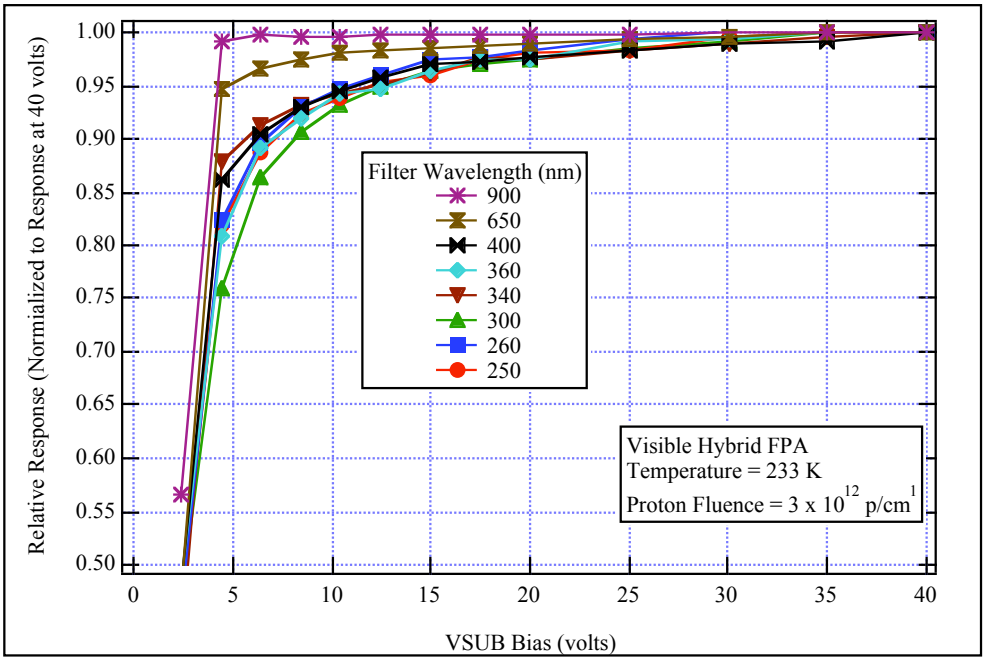

Figure 9. Normalized Response versus Substrate Bias at Several Wavelengths.

4.1.2. DARK CURRENT VERSUS PROTON FLUENCE

The FPA dark current was measured at a detector bias of 15 V at each proton fluence level. The median FPA dark current at each detector bias, are shown in Figure 10 as a function of proton fluence. These data show that the dark current increases, approximately linearly with proton fluence, approximately two orders of magnitude from pre-radiation measurements to a proton fluence of 3 x 10^{12} p/cm^2. At the completion of the radiometric characterization after achieving the maximum proton fluence, the FPA was maintained at 233 K in an un-biased state. After a 34 hour time period, the dark current was re-measured and was found to have decreased as shown by the data point identified by the blue square in Figure 10. The significant decrease in the dark current with time suggests that the dark current damage is being annealed. These data may suggest that the increase in dark current can be attributed to multiple effects: the first effect is the expected increase due to displacement effects in the detector structure, the second effect is unexpected and is possibly due to surface charging effects in the detector structure. It is possible that the number of surface states increases with increasing total ionizing dose resulting in the dramatic increase in dark current due to ionization effects. The annealing of the dark current is most likely a decrease in the dark current that is from the detector surface effects.

The visible hybrid FPA dark current distribution, measured at a proton fluence of 3 x 10^{12} p/cm^2, is shown in Figure 11. This distribution exhibits a long tail to the dark current distribution that is typically observed in Si detectors irradiated with protons. However, this increase in the dark current non-uniformity is not spatially distributed in a random manner across the detector array as is typically observed for proton interactions. Instead, the increase in detector dark current tends to be located around the perimeter of the detector array as is demonstrated in the 2-D map of the detector dark current at a proton fluence of 3 x 10^{12} p/cm^2 shown in Figure 12. The increase in dark current at the edge of the detector array is likely related to a change in the detector bias across the array, which will be shown to have a significant effect on the detector dark current.

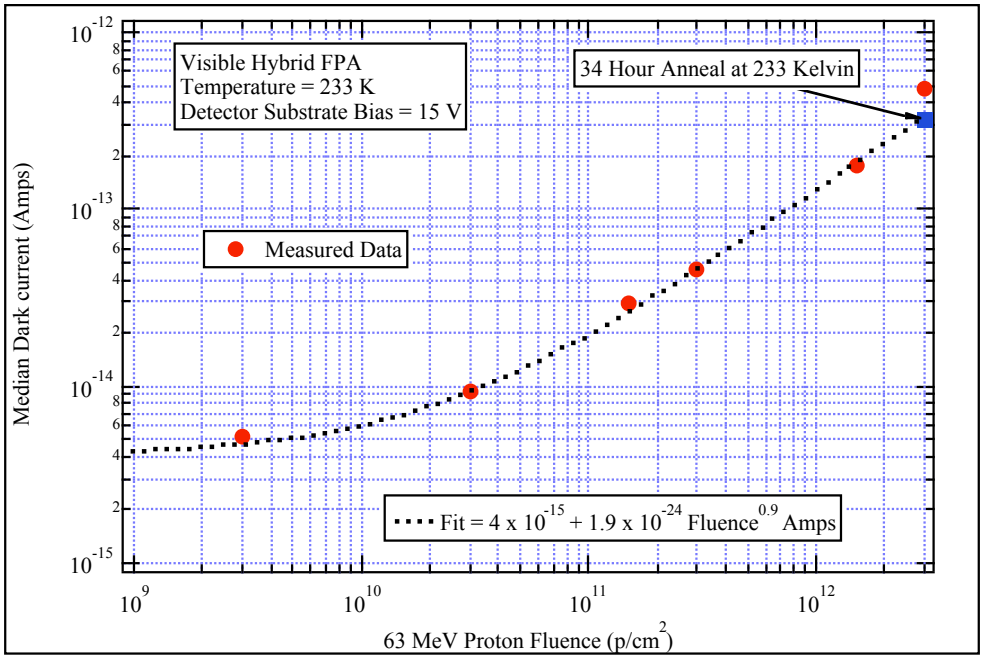

Figure 10. Median Dark Current versus Proton Fluence

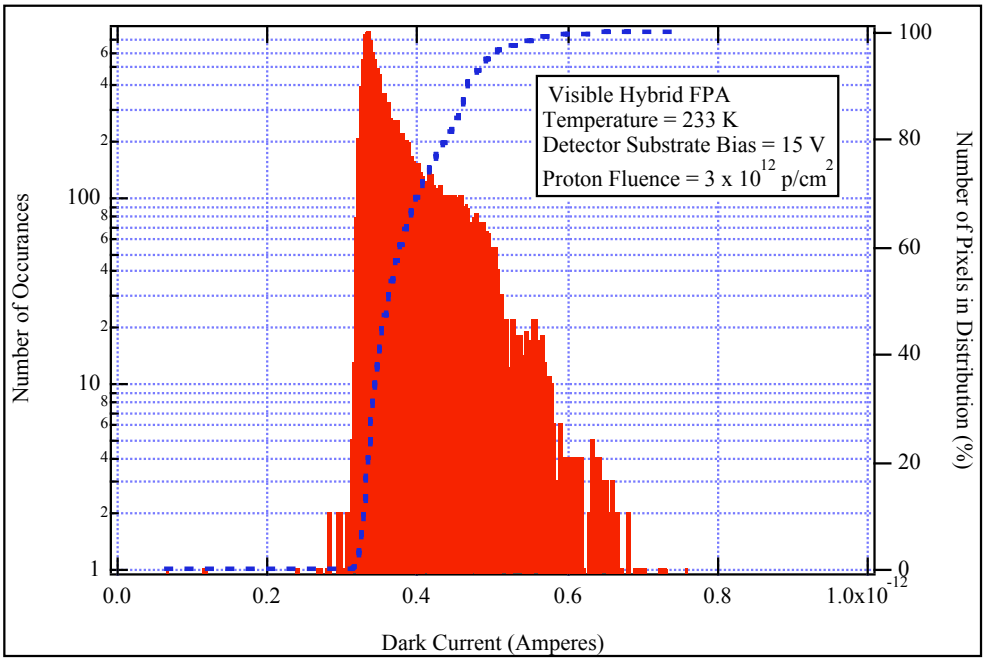

Figure 11. Dark Current Distribution at Proton Fluence = 3 x 10^{12} p/cm^2.

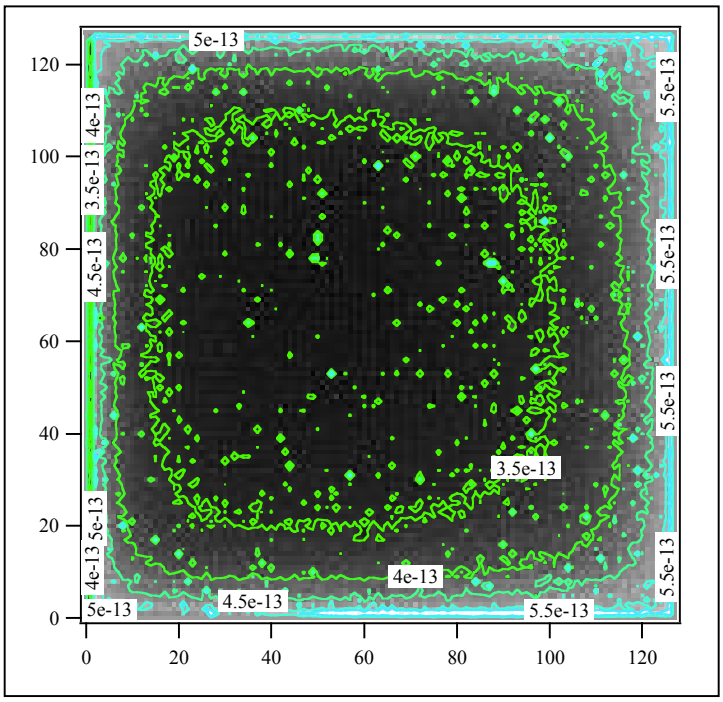

Figure 12. Dark Current Map at Proton Fluence = 3 x 10^{12} p/cm^2.

4.2. VISIBLE HYBRID FPA TOTAL IONIZING DOSE CHARACTERIZATION DATA

The operational and radiometric performance of the visible hybrid FPA was also characterized as a function of total ionizing dose. Total ionizing dose measurements were performed at the AFRL 5,300 Curie Cobalt-60 (^{60}Co) source located at Kirtland Air Force Base, NM. Prior to the total ionizing dose exposure, dosimetry measurements were made to determine the dose rate at the surface of the FPA using a calibrated ionization gauge placed inside the Dewar at the location of the FPA. The dose rate used for accumulating total ionizing dose was approximately 160 rad(Si)/minute. The FPA was fully biased and operational at 233 K during irradiation and during the extent of the total ionizing dose experiment.

4.2.1. FPA Radiometric Characterization Versus Total Ionizing Dose

The radiometric performance of the FPA was characterized as a function of total ionizing dose. Significant results observed were: (1) some very slight change in the FPA responsivity; (2) a shift in the nominal pixel dc output level; (3) minor changes in the noise level; (4) an increase in the NEI non-uniformity at low photon irradiance levels and (5) a dramatic increase in the detector dark current. The radiometric performance as a function of total ionizing dose is summarized in Figure 13, which plots pre-radiation, and 300 krad(Si) responsivity histograms and cumulative pixel distributions. The responsivity histograms show a < 5 % change in the median FPA responsivity at 300 krad(Si). This responsivity variation between pre-radiation and 300 krad(Si) could be attributed to variations in the experimental setup. NEI distributions measured pre-radiation and at 300 krad(Si) at photon irradiance levels of E_q = 6.3 x 10^{12} and 6.0 x 10^{12} ph/s-cm^2 are shown in Figure 14. These NEI data indicate that the FPA sensitivity was effectively unchanged at a total ionizing dose level of 300 krad(Si) when measured at relatively short integration time of 10.14 ms. The interesting aspect of these data is the slight increase in the tail of the NEI distribution measured at a low photon irradiance at 300 krad(Si). These data provide an early indication of an increase in the detector dark current non-uniformity with increasing total ionizing dose.

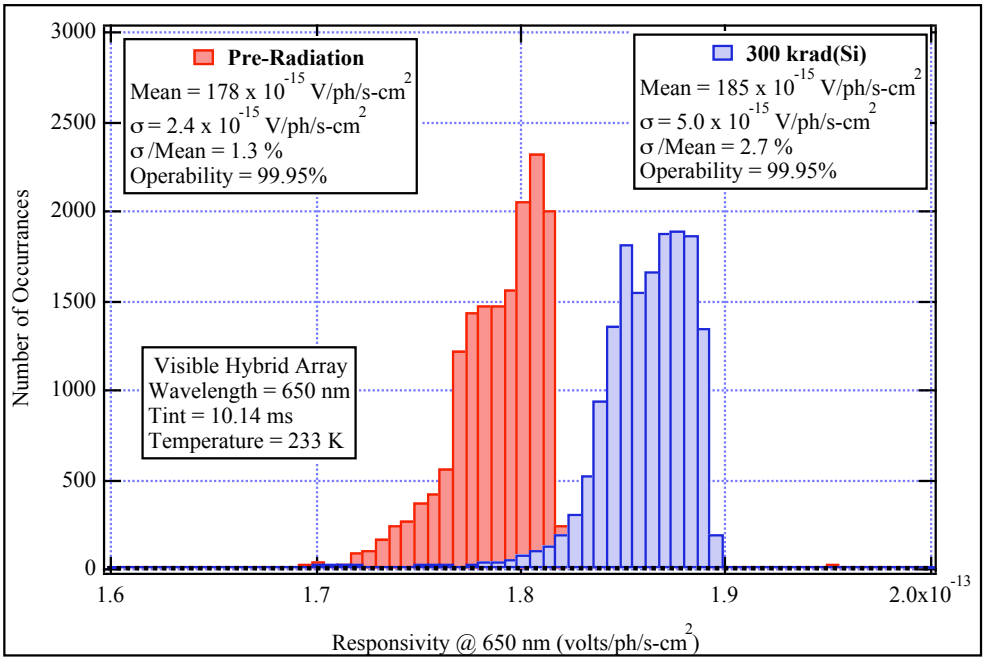

Figure 13. Responsivity Histograms, Pre-Radiation and 300 krad(Si)

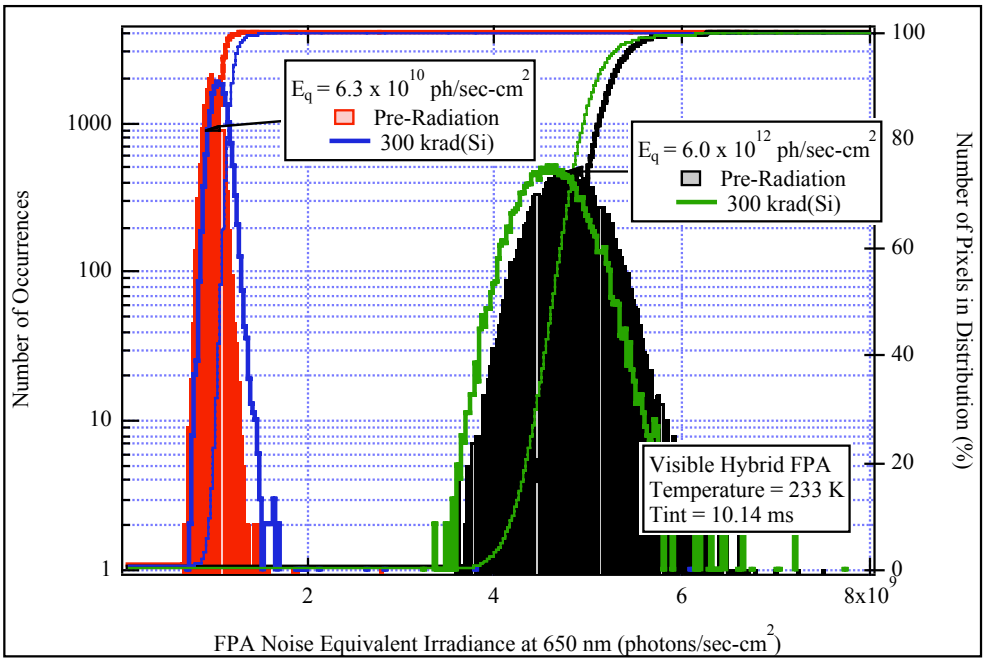

Figure 14. NEI Histograms, Pre-Radiation and 300 krad(Si).

4.2.2. DARK CURRENT VERSUS TOTAL IONIZING DOSE

The FPA dark current was measured at several detector biases (5, 10, 15, 20, and 25 V) at each total ionizing dose level. The median FPA dark current at each detector bias, are shown in Figure 15 as a function of total ionizing dose. The dark current unexpectedly increases with total ionizing dose, and at a total ionizing dose level of 750 krad(Si), the dark current at a detector bias of 15 V has increased by a factor of three hundred and twenty-five (325) from its pre-radiation level. The rate of dark current increase is a strong function of detector bias and the increase is most dramatic at the

higher detector biases. The rate of increase in dark current as a function of total ionizing dose is shown in Figure 16 that plots the ratio of the dark current at 750 krad(Si) to the pre-radiation dark current. This unexpected increase in dark current is likely a surface phenomenon in the detector structure. There is a very low probability that the increase is due to an increase in the dark current from the bulk of the Si detector structure. More likely, the surface of the detector is not pinned and the number of surface states increases with increasing total ionizing dose resulting in the dramatic increase in dark current.

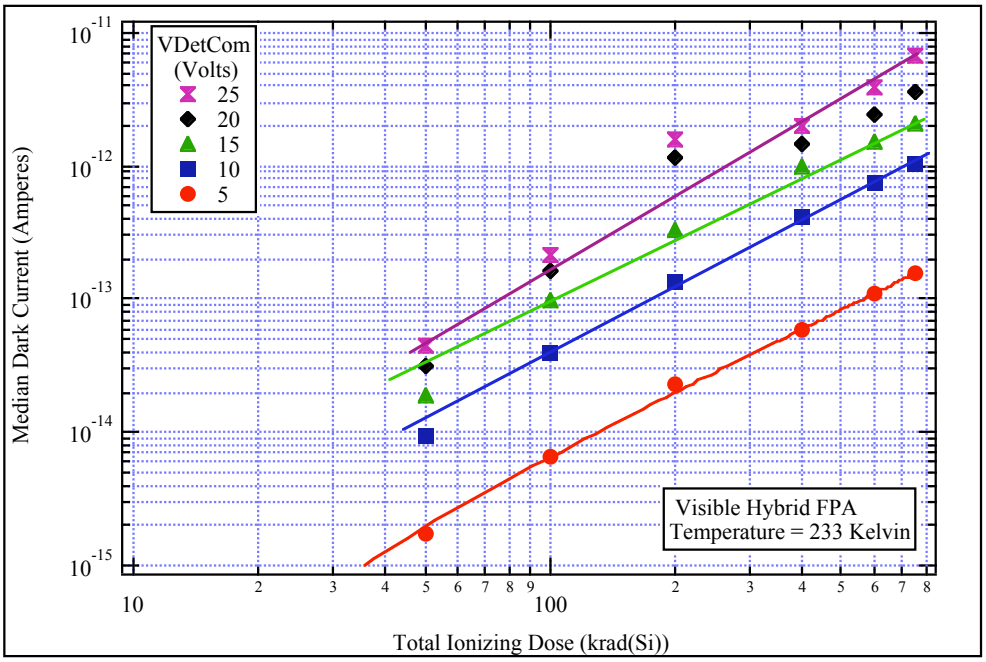

Figure 15. Median Dark Current versus Total Ionizing Dose at Several Detector Biases.

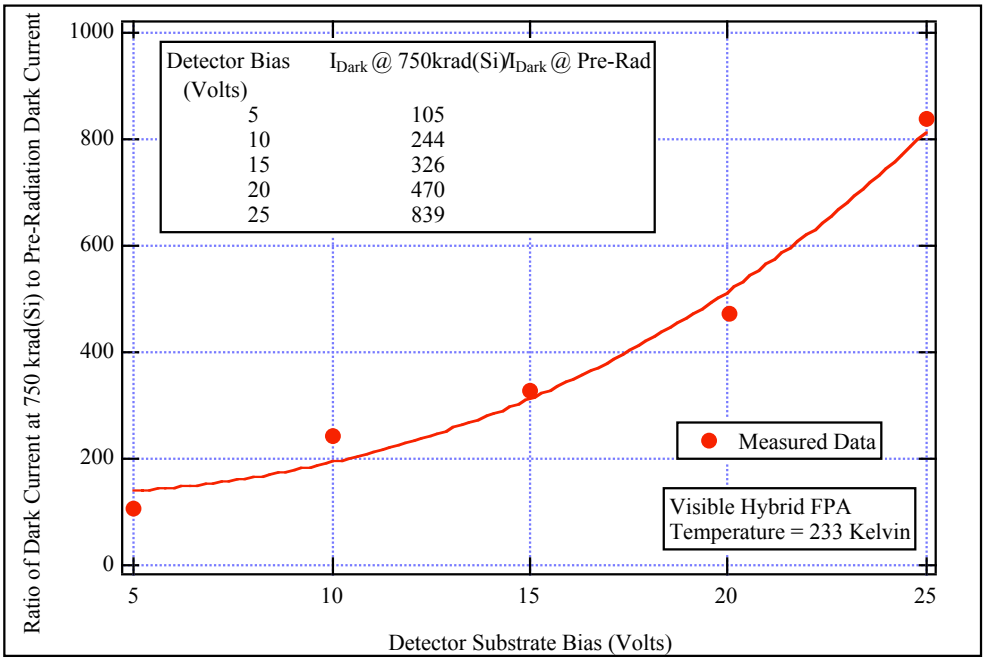

Figure 16. Dark Current Increase versus Detector Bias.

Dark current histograms, shown as a function of total ionizing dose in Figure 17, demonstrate an overall increase in dark current with increasing total ionizing dose. In addition; a tail to the dark current distribution develops at the lowest measured total ionizing dose level. An increase in the dark current non-uniformity is typically observed with increasing radiation in a proton environment; however, it is not usually an effect observed under ionizing radiation. This increase in non-uniformity is not a spatially random process; instead, the dark current increases more at the edges of the detector array as shown in Figure 18 that plots the two-dimensional dark current maps measured pre-radiation and at 750 krad(Si). Note that the increase in dark current at the edge of the detector array was observed during pre-radiation measurements. This increase is likely related to a change in the detector bias across the array, which has been shown to have a significant effect on the detector dark current (See Figure 16). The statistics associated with these dark current distributions are given in Table 2.

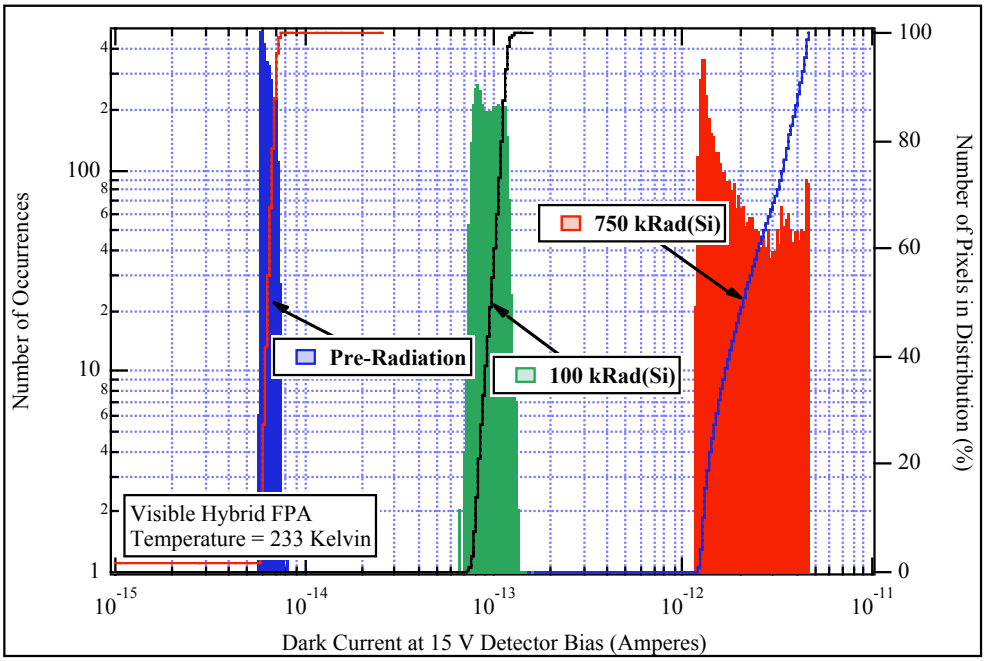

Figure 17. Dark Current Histograms versus Proton Fluence.

Table 2. Dark Current Distribution Statistics versus Total Ionizing Dose.

Total Ionizing Dose (krad(Si))	Median Dark Current (Amperes)	Standard Deviation of Dark Current Distribution (Amperes)	Dark Current Distribution Non-Uniformity (σ/Mean) (%)
Pre-Radiation	6.4×10^{-15}	4.7×10^{-15}	7
100	9.7×10^{-14}	1.3×10^{-14}	13
750	2.4×10^{-12}	1.1×10^{-12}	44

5. SUMMARY

Data have been presented that describe radiometric performance of visible Si P-i-N hybrid FPAs as functions of proton fluence and total ionizing dose. The radiometric performance of these devices is representative of the current performance level for radiation hardened visible hybrid FPAs operating at reduced operating temperatures. The pre-radiation performance approaches BLIP operation above a photon irradiance level of 2×10^{11} photons/sec-cm^2, with a median detector quantum efficiency of approximately 79% at 0.65 µm. The median detector exhibited low dark current and correspondingly low detector thermal and 1/f noise at a temperature of 233 K. The operability (in terms of the responsivity) was greater than 99.8% with an uncorrected non-uniformity of less than 1.3% (σ/mean).

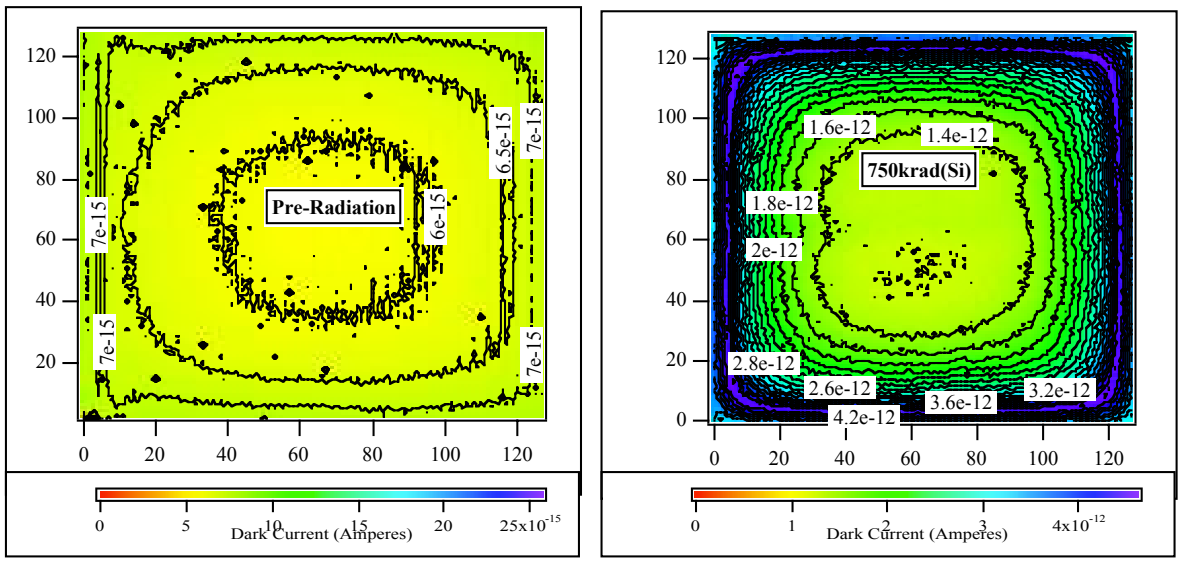

Figure 18. Dark Maps at Pre-Radiation and 750 krad(Si).

Two focal plane arrays were characterized using proton radiation that produces both displacement and ionizing damage to the FPAs. Operational and performance data were obtained on both devices as a function of proton fluence using 63 MeV protons. No appreciable change in responsivity was observed up to a proton fluence of 3 x 10^{12} p/cm^2 (400 krad(Si) of total ionizing dose). The median dark current increased approximately 2 orders of magnitude at a proton fluence of 3 x 10^{12} p/cm^2; this increase in dark current is a significant performance issue as the FPA is operated at longer integration times.

Two focal planes were also characterized using Cobalt-60 radiation to produce total ionizing dose damage to the FPAs. Operational and performance data were obtained on both devices as a function of total dose up to a dose of 750 krad(Si). No appreciable change in responsivity was observed up to a dose of 750 krad(Si). An unexpected increase in dark current was observed with increasing total ionizing dose in the Si P-i-N detectors. The median dark current increased more than two orders of magnitude from pre-radiation to 750 krad(Si), and it was found to be a strong function of detector bias. Since the optical response was not a function of bias, it is hypothesized that the dark current is a surface effect. Improvements in the detector design and processing can likely mitigate this effect.

6. ACKNOWLEDGEMENTS

The work reported in this paper was funded by the NASA Cross Enterprise Technology Development Program and was managed by Ball Aerospace & Technologies Corp.. We gratefully acknowledge the excellent support provided by the NASA Electronic Parts and Packaging Program (NEPP) by providing us with beam time at the Crocker Nuclear Laboratory. In particular, we acknowledge the support from Paul Marshall and Cheryl Marshall in helping with the radiation characterization of these visible focal plane arrays at the Crocker Nuclear Laboratory.

7. REFERENCES

1. C. J. Marshall and P. W. Marshall, "*Proton effects and test issues for satellite designers, part B: displacement damage effects*", 1999 IEEE NSREC Short Course Notes, pp. IV-50-IV-110.
2. G. R. Hopkinson, C. J. Dale, and P. W. Marshall, "*Proton effects in CCDs*", IEEE Trans. Nucl. Sci., vol. 43, no. 2, pp 614-627, Apr 1996.
3. J. C. Pickel, A. H. Kalma, G. R. Hopkinson, and C. J. Marshall, "*Radiation effects on photonic imagers – a historical perspective*",IEEE Trans. Nucl. Sci., vol. 50, no. 3, pp. 671-688, Jun 2003.
4. C.M. Castaneda, "*Crocker Nuclear Laboratory (CNL) Radiation Effects Measurement and Test Facility*", 2001 IEEE Radiations Effects Data Workshop, pp 77-81, IEEE (2001).